



Bacterial endotoxin (lipopolysaccharide) binds to the surface of gold nanoparticles, interferes with biocorona formation and induces human monocyte inflammatory activation

Yang Li, Zhenzhen Shi, Isabella Radauer-Preiml, Ancuela Andosch, Eudald Casals, Ursula Luetz-Meindl, Macarena Cobaleda, Zhoumeng Lin, Majid Jaber-Douraki, Paola Italiani, Jutta Horejs-Hoeck, Martin Himly, Nancy A. Monteiro-Riviere, Albert Duschl, Victor F. Puentes & Diana Boraschi

To cite this article: Yang Li, Zhenzhen Shi, Isabella Radauer-Preiml, Ancuela Andosch, Eudald Casals, Ursula Luetz-Meindl, Macarena Cobaleda, Zhoumeng Lin, Majid Jaber-Douraki, Paola Italiani, Jutta Horejs-Hoeck, Martin Himly, Nancy A. Monteiro-Riviere, Albert Duschl, Victor F. Puentes & Diana Boraschi (2017) Bacterial endotoxin (lipopolysaccharide) binds to the surface of gold nanoparticles, interferes with biocorona formation and induces human monocyte inflammatory activation, *Nanotoxicology*, 11:9-10, 1157-1175, DOI: [10.1080/17435390.2017.1401142](https://doi.org/10.1080/17435390.2017.1401142)

To link to this article: <https://doi.org/10.1080/17435390.2017.1401142>



© 2017 The Author(s). Published by Informa UK Limited, trading as Taylor & Francis Group.



[View supplementary material](#)



Published online: 01 Dec 2017.



[Submit your article to this journal](#)



Article views: 1414








[View Crossmark data](#)



Citing articles: 10 [View citing articles](#)

Bacterial endotoxin (lipopolysaccharide) binds to the surface of gold nanoparticles, interferes with biocorona formation and induces human monocyte inflammatory activation

Yang Li^{a,b,c,d} , Zhenzhen Shi^e , Isabella Radauer-Preiml^f, Ancuela Andosch^f, Eudald Casals^{g,h}, Ursula Luetz-Meindl^f, Macarena Cobaleda^{g,h}, Zhoumeng Lin^e , Majid Jaber-Douraki^e, Paola Italiani^a, Jutta Horejs-Hoek^f, Martin Himly^f, Nancy A. Monteiro-Riviere^b , Albert Duschl^f, Victor F. Puntès^{g,h,i} and Diana Boraschi^a 

^aInstitute of Protein Biochemistry, National Research Council, Napoli, Italy; ^bNanotechnology Innovation Center of Kansas State University (NICKS), Department of Anatomy and Physiology, Kansas State University, Manhattan, KS, USA; ^cGuangdong Key Laboratory of Nanomedicine, Institute of Biomedicine and Biotechnology, Shenzhen Institutes of Advanced Technology (SIAT), Chinese Academy of Sciences, Shenzhen, China; ^dCollege of Life Science, Hebei Normal University, Shijiazhuang, Hebei, China; ^eInstitute of Computational Comparative Medicine (ICCM), Department of Anatomy and Physiology, Kansas State University, Manhattan, KS, USA; ^fDepartment of Molecular Biology, University of Salzburg, Salzburg, Austria; ^gInstitut Català de Nanotecnologia (ICN), Bellaterra, Spain; ^hVall d'Hebron Research Institute (VHIR), Barcelona, Spain; ⁱInstitut Català de Recerca i Estudis Avançats (ICREA), Barcelona, Spain

ABSTRACT

Nanoparticles (NPs) are easily contaminated by bacterial endotoxin (lipopolysaccharide [LPS]). The presence of LPS can be responsible for many immune/inflammatory effects attributed to NPs. In this study, we examined the effects of LPS adsorption on the NP surface on the formation of a biocorona in biological fluids and on the subsequent inflammation-inducing activity of NPs. Different gold (Au) NPs with sizes ranging from 10 to 80 nm and with different surface functionalization (sodium citrate, lipoic acid, and branched polyethyleneimine (BPEI), or polyethylene glycol (PEG)) were exposed to *E. coli* LPS under different conditions. The binding capacity of LPS to the surface of AuNPs was dose- and time-dependent. LPS attached to sodium citrate and lipoic acid coatings, but did not adhere to BPEI- or PEG-coated NPs. By computational simulation, the binding of LPS to AuNPs seems to follow the Langmuir absorption isotherm. The presence of LPS on AuNP surface interfered and caused a decrease in the formation of the expected biomolecular corona upon incubation in human plasma. LPS-coated AuNPs, but not the LPS-free NPs, induced significant inflammatory responses *in vitro*. Notably, while free LPS did also induce an anti-inflammatory response, LPS bound to NPs appeared unable to do so. In conclusion, the unintentional adsorption of LPS onto the NP surface can affect the biocorona formation and the inflammatory properties of NPs. Thus, for an accurate interpretation of NP interactions with cells, it is extremely important to be able to distinguish the intrinsic NP biological effects from those caused by biologically active contaminants such as endotoxin.

ARTICLE HISTORY

Received 3 May 2017
Revised 8 September 2017
Accepted 27 October 2017



KEYWORDS


Nano-immunosafety; endotoxin contamination; biocorona modulation; gold nanoparticles; inflammatory effects

Introduction

Due to the increased usage of nanomaterials for different applications, the safety aspects are of key importance for ensuring their responsible use and for sustaining their industrial development (Savolainen et al. 2013). Nanosafety studies depend on scientific reports on the biological effects of nanoparticles (NPs) in living organisms, in order to predict and correct the possible deleterious impact

on human and environmental health. Many studies showed that NPs may have adverse effects on health, mainly due to their small size, large surface area per mass and highly reactive properties (Bastús et al. 2008; Ge et al. 2012; Li et al. 2012; Wang et al. 2013). Among the different NP effects in biological systems, activation of immune responses is considered a central element for assessing health risks of NPs (Boraschi and Duschl 2012; Li et al. 2016).

CONTACT Yang Li  yang.li.nano@gmail.com  Guangdong Key Laboratory of Nanomedicine, Institute of Biomedicine and Biotechnology, Shenzhen Institutes of Advanced Technology (SIAT), Chinese Academy of Sciences, Shenzhen 518055, China

 Supplemental data for this article can be accessed [here](#).

© 2017 The Author(s). Published by Informa UK Limited, trading as Taylor & Francis Group. This is an Open Access article distributed under the terms of the Creative Commons Attribution-NonCommercial-NoDerivatives License (<http://creativecommons.org/licenses/by-nc-nd/4.0/>), which permits non-commercial re-use, distribution, and reproduction in any medium, provided the original work is properly cited, and is not altered, transformed, or built upon in any way.

Reliability of the safety assays, both *in vitro* and *in vivo*, implies the accurate characterization of the nanomaterial being tested, which should be devoid not only of chemical impurities but also of biologically active contaminants (Dobrovolskaia, Germolec, and Weaver 2009; Li and Boraschi 2016). In this context, the presence of an ubiquitous contaminant such as bacterial endotoxin (lipopolysaccharide, LPS) should be thoroughly assessed in newly developed engineered NP preparations, since LPS is a robust, persistent, ubiquitous, potent immune/inflammatory activator, and toxic molecule, which is difficult to detect in NPs (Li et al. 2015) and could be responsible for the majority of inflammatory/toxic effects generally attributed to engineered NPs (Li and Boraschi 2016; Li, Fujita, and Boraschi 2017).

LPS is a major component of the outer cell membrane of gram-negative bacteria, which potently induces an inflammatory response in cells that express Toll-like receptor 4 (TLR4). LPS binds to the LPS-binding protein (LBP), which facilitates the engagement with TLR4 and the formation of the complex with CD14 and MD2, thereby initiating cell activation. TLR4 is expressed on many cell types but the most reactive cells are monocytes and macrophages, which in response to LPS are activated (M1 or classical activation) to become cytotoxic and to produce a variety of inflammatory factors such as interleukin (IL)-1 β , IL-6, IL-8, and tumor necrosis factor (TNF)- α (Li and Boraschi 2016). LPS can also be found in the absence of live bacteria, and is present in most chemicals and glassware in the laboratory because it is heat stable and cannot be eliminated by sterilization methods (Gorbet and Sefton 2005; Li and Boraschi 2016). In previous studies, we showed that different batches of NPs synthesized following an identical protocol may have different contamination levels of endotoxin depending on the level of cleanliness during the synthesis procedure (Oostingh et al. 2011). Also, we found that poor handling processes and storage under different conditions can contaminate NPs and endow them with an inflammatory potential (Murali et al. 2015). This is a consequence of the fact that LPS can bind to all kinds of surfaces and thus represents a ubiquitous contaminant in all types of biomaterials (Gorbet and Sefton 2005; Li and Boraschi 2016). Darkow et al. showed that endotoxin can bind to

different surface-functionalized NPs, depending on the NP ability to establish Coulomb and van der Waals interactions with the endotoxin molecules (Darkow et al. 1999). It has been reported that the hydrophobic part of LPS (lipid A) binds to the surface of latex particles, so that the resulting LPS-coated particles could be used for agglutination immunoassays (Peula-García et al. 2002). Another study showed that cobalt-based NPs have a strong affinity for lipid A and suggested to use these NPs for the elimination of *E. coli* bacteria from suspensions (Bromberg et al. 2010). Although many studies have shown the interaction of LPS with NPs and used this feature to develop new technical applications, less attention has been given to the influence of LPS contamination for nanosafety assessment. Even in the field of nanomedicine, this topic has been underestimated and there are numerous publications on the biological and immunological effects of NPs in which LPS contamination was not assessed.

In this study, a set of different gold (Au) NPs, spanning a size range between 10 and 80 nm and with different surface functionalization was used to investigate the interaction between LPS and NPs and the consequent effects on biomolecular corona formation. A computational method to simulate the interaction between LPS and the Au NP surface was also employed, in which we incorporated the acquired experimental data to define a mathematical relationship between LPS and the Au NPs. The goal of this study was to determine the inflammation-inducing capacity of LPS-coated NPs on human monocytes in culture, and to compare it to uncoated NPs and to free LPS.

Methods

Types of Au NPs used in this study

Sodium citrate-coated 10 nm Au NPs (Au10CIT) were synthesized by the wet chemistry method under conditions that enabled the collection of stable and narrowly dispersed NPs (Figure 1). Citrate-coated 50 nm Au NPs were purchased from Sigma-Aldrich Inc. (St. Louis, MO, USA). The 40 nm and 80 nm lipoic acid (Au40LIP and Au80LIP), 40 nm branched polyethyleneimine (Au40BPEI), and 40 nm polyethylene glycol (Au40PEG)-coated Au NPs were custom-synthesized by nanoComposix, Inc. (San Diego, CA, USA). Since the commercial citrate-coated 50 nm Au NPs fell in the

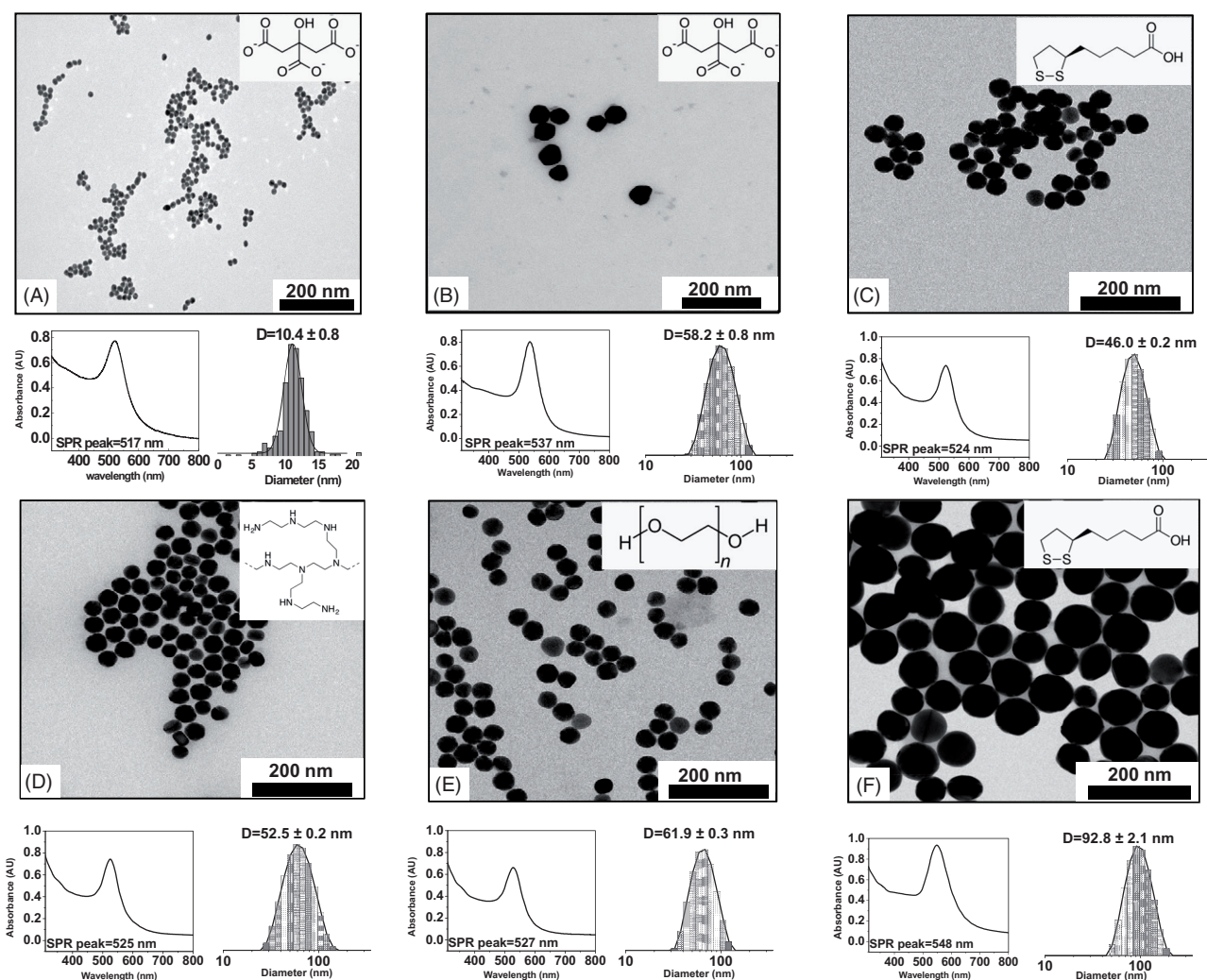


Figure 1. Characterization of Au NPs. TEM, UV-VIS spectra and size distribution of the different types of Au NPs. (A) Au10CIT, (B) Au40CIT, (C) Au40LIP, (D) Au40BPEI, (E) Au40PEG, and (F) Au80LIP. In the upper right corners are shown the chemical formulas of citrate (A and B), lipoic acid (C and F), BPEI (D), and PEG (E).

Table 1. Characteristics of Au NPs.

Name	Hydrodynamic diameter (nm)	pH	Stock concentrations			Z-potential (mV)	Surface coating	LPS content (EU/ml)
			$\mu\text{g/ml}$	NPs/ml	cm^2/ml			
Au10CIT	10.4 ± 0.8	7	32	3.0×10^{12}	10	-67	Sodium citrate	0.45
Au40CIT	58.2 ± 0.8	7	1.14	3.5×10^{10}	2.7	-42	Sodium citrate	20
Au40LIP	46.0 ± 0.2	6	1080	1.6×10^{12}	82	-42	Lipoic acid	<2.5
Au40BPEI	52.5 ± 0.2	7	1060	1.7×10^{12}	81	67	BPEI	<2.5
Au40PEG	61.9 ± 0.3	6	1010	1.4×10^{12}	75	-4.7	PEG	<2.5
Au80LIP	91.1 ± 1.1	7	1060	1.9×10^{11}	39	-45	Lipoic acid	<2.5

40–60 nm size range of all the other 40 nm Au NPs, we defined them as Au40CIT. The detailed characteristics are shown in Figure 1 and Table 1.

Au NP synthesis

The synthesis of Au10CIT was carried out starting with metallic salt precursors either decomposed

or reduced in the presence of stabilizers. Reagents were purchased from Sigma-Aldrich Inc., and used as received. In detail, Au10CIT were obtained based on Turkevich *et al.* (Turkevich, Stevenson, and Hillier 1955), *i.e.*, by fast addition of 1 ml hydrogen tetrachloroaurate (HAuCl_4) 0.025 M to 150 ml of boiling trisodium citrate (SC) 2.2×10^{-3} M under vigorous stirring. After 3–5 min, NPs

developed a characteristic red color of the colloidal gold and the solution was cooled down to room temperature (RT). The resulting NPs were loosely coated with negatively charged citrate anions acting as stabilizers. The Au40CIT were purchased from Sigma-Aldrich Inc., and synthesized based on Bastús *et al.* (Bastús, Comenge, and Puntès 2011). The other 40 nm and 80 nm Au NPs were obtained from nanoComposix Inc., and their synthesis methods were reported previously (Choi, Riviere, and Monteiro-Riviere 2016; Li and Monteiro-Riviere 2016).

Au10CIT were synthesized using endotoxin-free conditions (endotoxin-free water, depyrogenated glassware), in order to minimize endotoxin contamination of NPs (Li and Boraschi 2016). The endotoxin contamination level of Au NPs was evaluated with optimized procedures (see below).

NP characterization

NPs were fully characterized by different techniques, *i.e.*, transmission electron microscopy (TEM), zeta potential (Z-potential), dynamic light scattering (DLS) and *UV-visible spectrophotometry* (UV-VIS).

Transmission electron microscopy (TEM)

TEM micrographs were acquired with a JEOL 1010 electron microscope at an accelerating voltage of 80 kV. Samples for TEM were prepared by drop casting on carbon-coated copper grids, then dried at RT. Different areas of the grid were observed with different magnifications, and more than 400 NPs were computer-analyzed and measured for size distribution.

LPS binding on the surface of Au NPs was characterized by TEM. Samples were placed on the coated copper grids directly after incubation and examined unstained on a FEI Tecnai G2 Spirit BioT - WIN TEM at an accelerating voltage of 120 kV.

Z-potential measurement and DLS

Measurements were made with a Malvern ZetaSizer Nano ZS (Malvern Instruments, Malvern, Worcestershire, UK) operating at a light source wavelength of 532 nm and a fixed scattering angle of 173°, on 0.8 ml aliquots of the colloidal NP suspensions. The software was set with specific

parameters of refractive index and absorption coefficient of NP material and solvent viscosity, required to obtain the correct value for each type of NP. Zeta-potential (surface charge) measurements were used to determine the stability of a colloidal suspension of electrostatically stabilized NPs. Conversely, DLS allows the determination of the hydrodynamic diameters of colloidal particles and conjugates, *i.e.*, the diameter of the sphere with the same Brownian motion as the particle under analysis.

UV-Visible Spectrophotometry (UV-VIS)

UV-VIS spectra were acquired with a Shimadzu UV-2400 spectrophotometer, on 1 ml aliquots of the NP suspension, and performing the spectral analysis in the 300-800 nm range. This technique is used for metallic NPs that exhibit a characteristic absorbance maximum in the visible range (the surface plasmon resonance, SPR), which changes depending on the size and surface alterations. However, all materials used absorb light in the visible or UV range, making these measurements appropriate in all cases.

Endotoxin adhesion to NPs and interference with biomolecular corona formation

One ml of the Au10CIT stock solution (32 µg/ml) was exposed to different concentrations (0.3, 1.0, 3.3, and 10.0 µg/ml) of LPS from *E. coli* LPS O55:B5 (cat. n. L6529, Sigma-Aldrich Inc.) at different temperatures (4 °C, RT and 37 °C) at different time points. Au10CIT were collected by ultracentrifugation at 36000 × g for 40 min. Two washing steps were performed with endotoxin-free water to eliminate the unbound LPS. One ml Au40CIT (3.5 × 10⁵ NPs/ml) was incubated with 5 µg *E. coli* LPS overnight at 4 °C. The excess bystander LPS was removed by three washing steps (5 min at 18000 rpm). One ml of Au40LIP, Au40BPEI, Au40PEG, or Au80LIP stock solutions (25 µg/ml) were incubated with 1.0, 3.3, 10.0 µg/ml *E. coli* LPS over time (up to 1 week), collected at 14000 × g for 10 min, and washed in endotoxin-free water to eliminate unbound LPS. Characteristics of these NP were evaluated by UV-VIS, DLS, and TEM before and after exposure to LPS.

For analysis of potential interference of LPS with biomolecular corona formation, 25 µg/ml LPS-coated Au40LIP (previously incubated with 10 µg/ml *E. coli*

LPS for 2 h at RT and washed) were resuspended in pooled human plasma that collected from healthy donors ($n=5$) (Biological Specialty Corporation, PA, USA) and incubated at 37 °C over time, and the size variation due to the corona formation was analyzed by DLS. For specifically investigating the formation of a stable biomolecular corona, after 4 h incubation with plasma at 37 °C, NPs were centrifuged at 4 °C at 14000 \times g for 10 min and resuspended in PBS for DLS characterization.

Sodium dodecyl sulfate polyacrylamide gel electrophoresis (SDS-PAGE) analysis of biomolecular corona proteins

Au40LIP (25 μ g/ml) were incubated with or without 10 μ g/ml LPS for 2 h at RT and washed with endotoxin-free water as described. After two washings, LPS-coated and uncoated Au NPs were resuspended in 500 μ l of human plasma either undiluted (100%) or diluted in PBS at 10% or 55%. After 4 h at 37 °C, the NPs were centrifuged at 14000 \times g for 10 min at 4 °C, the pellets were resuspended in PBS, washed twice and resuspended in 90 μ l PBS. Then 30 μ l 4 \times Laemmli sample buffer (Bio-Rad Laboratories, Inc., Hercules, CA, USA) were added and incubated at 95 °C for 5 min. An equal sample volume (10 μ l) was loaded in 4%-12% polyacrylamide gel (Mini-PROTEAN® TGX™ precast gels, Bio-Rad Laboratories, Inc.). Gel electrophoresis was performed at 120 V for 60 min. The gels were stained with the Coomassie brilliant blue R-250 staining solution (Bio-Rad Laboratories, Inc.) for 2 h and destained overnight with the Coomassie brilliant blue R-250 destaining solution (Bio-Rad Laboratories, Inc.). Gel density was analyzed by image J.

CytoViva characterization of LPS binding on the Au NP surface

For analysis of LPS binding to the Au NP surface, optical and hyperspectral imaging analysis were acquired with a dark field-based optical illumination system from CytoViva (CytoViva Inc., Auburn, AL, USA). Au NPs and LPS-coated Au NPs were applied to a slide and covered with a coverslip (Carl Roth GmbH Co KG, Karlsruhe, Germany). The measurement is based on the characteristic scattering profile of Au NPs. Each pixel of the image was recorded at a wavelength of 400-1000 nm, and was automatically

compared by the classification algorithm spectral angle mapper (SAM) to the LPS-coated Au NPs. The data is presented as normalized mean region of interest (ROI) of 1,100 LPS-coated Au NPs normalized to the mean ROI of 1,100 Au NPs.

Limulus amoebocyte lysate (LAL) assay

The endotoxin contamination of Au NPs was measured with the chromogenic LAL assay Pyrochrome® (Associates of Cape Cod, Inc., East Falmouth, MA, USA) or QCL-1000™ (Lonza Group Ltd., Basel, Switzerland), following the manufacturers' instructions. A newly established protocol for testing endotoxin in interference-free conditions was used (Li et al. 2015). Evaluation was performed on at least 3 different concentrations of NPs, previously tested for lack of interference with the assay's optical readout, and which had an acceptable value of recovery rate (assessed by running the positive product controls that evaluate the NP interference with the assay components). Briefly, 50 μ l NPs dilutions were mixed with 50 μ l LAL in 96-well plate, and incubated for 30 min or 10 min at 37 °C followed by addition of 50 or 100 μ l substrate solution. After incubation for 6-10 min at 37 °C, 100 μ l of the stop reagent (acetic acid, 25%v/v in water) was added to each well. For the Pyrochrome® assay, the diazo reagents (100 μ l in total) were applied to generate azo dye and shift the detection wavelength from 405 nm to 540 nm (to avoid the potential readout interference by NPs). Absorbance was measured at 405 nm or 540 nm with a plate reader (Tecan, Groedig, Austria) and was compared with the endotoxin standard curve (1 endotoxin unit [EU] approximately corresponding to 0.1-0.2 ng LPS).

Agent-based model (ABM) of interaction between LPS and Au NPs

We used NetLogo 5.3.1 (Netlogo 2014), a platform with a simplified programming environment, easily implemented tool sets, and well-established documentation support, to implement this ABM (Shi, Wu, and Ben-Arieh 2014; Shi et al. 2016). The primary user interface of NetLogo is comprised of two-dimensional (2D) grids, in which agents can be divided into two categories: "patches" and "turtles." "Patches" are fixed agents placed on background

grids in the model workspace. "Turtles" are mobile agents that can occupy a position or move freely on the surface of patches and execute certain functions or actions regulated by the simulated system (Shi et al. 2016). The interface of NetLogo allows a modeler to set initial parameters and observe simulation results. Both LPS and Au NPs are "turtles" in this simulation. The ABM was conducted on a high-end desktop (technical specification: DELL Intel i7-4790 3.6GHz with 16 GB of RAM).

Estimated mathematical relationship between SPR peak red-shift and the amount of LPS bound to Au NPs

Estimation of a mathematical relationship between the SPR peak of the UV-VIS spectrum and the amount of bound LPS on Au NPs was performed with the MATLAB software, using the Curve Fitting Toolbox. To estimate the amount of LPS bound to Au10CIT resulting in a SPR red-shift, a simulation was performed based on the observation that, at the LPS concentration of 10 µg/ml, binding to Au10CIT was saturated within 2 min. On this basis, 6,423 steps were calculated in the *in silico* simulation runs, corresponding to the 2 min saturation time in the above experiment.

Human monocyte isolation

Human peripheral blood mononuclear cells (PBMC) were separated from buffy coats of healthy donors by centrifugation with Ficoll-Paque PLUS (GE Healthcare, Bio-Sciences AB, Uppsala, Sweden). CD14⁺ monocytes were isolated from PBMC using the Monocyte Isolation kit II (Miltenyi Biotec, Bergisch-Gladbach, Germany) according to the manufacturer's protocol. The purity of the isolated monocytes (>98%) was determined by differential counts on cytocentrifuge smears stained with a modified Wright-Giemsa dye (Diff Quik®, Medion Diagnostics AG, Düringen, Switzerland). Viability was determined by trypan blue dye exclusion and always exceeded 98%.

Monocyte activation test (MAT)

Monocytes were cultured at a density of 2.5×10^6 cells/well in 12-well culture plates (Costar®, Corning

Inc.; New York, NY, USA) in 1 ml of RPMI 1640 + Glutamax-I medium (GIBCO® by Life Technologies, Paisley, UK) supplemented with 50 µg/ml Gentamicin (GIBCO®), 5% heat-inactivated human AB serum (Lonza Group Ltd.) at 37 °C in moist air with 5% CO₂.

LPS-coated/-uncoated Au NPs were preincubated with 100% heat-inactivated human AB serum and incubated for 4 h at 37 °C before addition to cells in culture. LPS-coated Au NPs were added to monocytes in culture at final concentrations between 0.25 and 2 cm²/ml. After 18 h, supernatants and cells were collected for analysis of protein production and gene expression.

Activation of NFκB-responsive reporter cells

Human embryonic kidney (HEK) 293 cells (Sigma-Aldrich Inc.) were plated at a density of 1.2×10^5 cells/well of 24-well plates (Corning Inc.) in 500 µl Dulbecco's Modified Eagle Medium (DMEM) (Sigma-Aldrich Inc.) supplemented with heat-inactivated 10% fetal calf serum (FCS), 2 mM L-glutamine and 2 mM nonessential amino acids (NEAAs), 100 U/ml penicillin and 100 µg/ml streptomycin. On the next day, the cells were transfected using the Lipofectamine 2000 reagent (Invitrogen, Life Technologies) according to the manufacturer's instructions. Briefly, 1.5 µl Lipofectamine 2000 reagent and a set of plasmid DNAs were diluted in 25 µl Opti-Mem (GIBCO®) per well. The plasmids used were pGL3Neo-NFκB-LUC (400 ng; kindly provided by Min Li-Weber (Li-Weber, Giasi, and Krammer 1998)), pCDNA3-CD14 (20 ng), pEFBOS-MD2 (20 ng), and pCDNA3-TLR4 (60 ng) (all kindly provided by Andrei Medvedev and Douglas Golenbock). The reactions were mixed, pooled, and incubated for 5 min at RT. After the incubation, 50 µl of the transfection mix were added to the wells. On the next day, the medium was filled up to 1 ml and cells were exposed to different concentrations of LPS, Au NPs, and LPS-coated Au NPs. LPS coating was obtained by incubating 1 ml of Au40 CIT NPs (3.5×10^{10} NPs) with 50 ng LPS overnight at 4 °C, and then collecting NPs by centrifuging 3 × 5 min at 18000 rpm to remove unbound LPS. After 24 h, the supernatants were collected and stored at -80 °C for cytokine ELISA, and cells were lysed with 100 µl/well of lysis buffer (100 mM

potassium phosphate pH 7.8, 0.1% Triton X-100, 1 mM dithiothreitol). The lysates were transferred to white polystyrene flat-bottom microtiter plates (Greiner Bio-One, Kremsmuenster, Austria), and the luciferase activity was measured with a plate reader (Tecan), after addition of 50 μ l of luciferase substrate per well.

RNA extraction and quantitative real-time polymerase chain reaction (RT-PCR) analysis

RNA was extracted by using Qiagen miRNeasy kit (Qiagen, Hilden, Germany) and quantified by ND-1000 spectrophotometer (NanoDrop Technologies, Wilmington, DE, USA). The RNA integrity was checked by microcapillary electrophoresis on Agilent 2100 Bioanalyzer (Agilent Technologies, Palo Alto, USA) on the basis of the ratio between 28S and 18S rRNA peak areas and of the RNA integrity number (RIN, >8) index. RNA samples were stored at -80°C until use.

cDNA was reverse-transcribed from total RNA (300 ng per sample) with oligo-dT and random primers, according to the QuantiTect Reverse Transcription Kit (Qiagen) instructions. Two to three separate reverse transcriptions were performed for each sample, and an identical reaction without reverse transcriptase was run as the negative control. Taqman quantitative PCR was performed with a Rotor-GeneTM 3000 (Corbett Research, Doncaster, Victoria, Australia), using the QuantiTect SYBR Green PCR Master Mix (Qiagen). The final reaction contained 12.5 μ l 2x Master Mix, 0.3 μ M of each primer, and 2.5 μ l of cDNA in a total volume of 25 μ l. PCR conditions were 94°C for 15 min, followed by 35-40 cycles of 94°C for 15 s, 50 - 60°C for 30 s, and 72°C for 30 s. Primer sequences were supplied by Qiagen both for target genes (*IL1B*, *IL1RN*) and housekeeping genes (*ACTB*). Relative gene expression was calculated using the efficiency correction method, which calculates the relative expression ratio from the quantitative PCR (qPCR) efficiencies and the C_t between the target gene and the endogenous control, relative to a calibrator sample (Pfaffl 2001).

Protein detection by ELISA

Human IL-1 β and IL-1Ra were measured in the cell culture supernatants by ELISA with commercially available kits (R&D Systems, Inc., Minneapolis, MN,

USA). Human IL-8 was measured by Human IL-8 Standard ELISA Development Kit from PeproTech (Rocky Hill, NJ, USA). Each sample was assayed in duplicate, and detection was performed with a microplate spectrophotometer (Tecan).

Statistical analysis

The results are expressed as mean \pm standard deviation (SD) of 3 independent experiments, calculated using Microsoft[®] Office Excel 2007 and analyzed using GraphPad Prism (GraphPad Software Inc., USA). Statistical analysis was performed using a one-way analysis of variance (one-way ANOVA) and a Tukey's *post hoc* test, or F-test and Student's t-test (as appropriate). *p*-Values <0.05 were regarded as statistically significant.

Ethics statement

No ethical approval or informed consent is required by the Italian law for discarded blood products. The use of the blood samples from anonymous healthy donors for the MAT was approved by the Ethical Committee of the University of Pisa S. Chiara Hospital (prot. AOUP 33998 of Sep. 29, 2006).

Result

Characteristics of Au NPs

Six different types of Au NPs were used in this study with different sizes and with different surface coatings. Sodium citrate-coated 10 nm and 40-60 nm Au NPs (Au10CIT and Au40CIT), lipoic acid-coated 40 nm and 80 nm Au NPs (Au40LIP and Au80LIP), 40 nm Au NPs coated with branched polyethyleneimine (Au40BPEI), and with polyethylene glycol Au NPs (Au40PEG) (Figure 1 and Table 1). The endotoxin contamination levels of these Au NPs were determined to be less than 2.5 EU/ml in their stock solutions (with contamination in Au10CIT as low as 0.45 EU/ml), except for the commercial Au40CIT that had an endotoxin contamination of 20 EU/ml (Table 1).

In the attempt of understanding whether and up to what extent endotoxin binds to the surface of NPs, and if the endotoxin on the NP surface may trigger inflammation, we performed a series of experiments for assessing both the features of endotoxin adsorption on the Au NPs surface and its

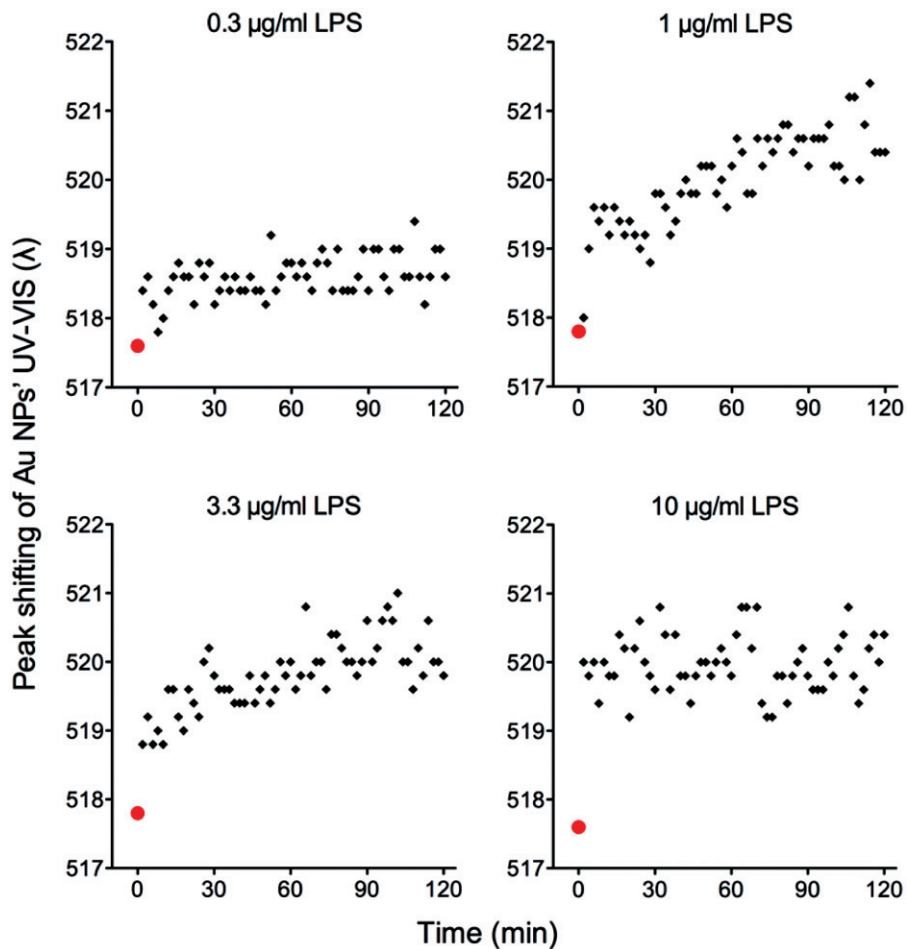


Figure 2. UV-VIS surface plasmon resonance spectrum red-shift of Au NPs after exposure to different concentrations of LPS. Au10CIT were incubated with different concentrations of *E. coli* LPS. Au NPs were characterized by UV-VIS at 2 min intervals for 2 h. The red point at time zero represents the value of untreated NPs.

capacity to interfere with the formation of a biomolecular corona in biological fluids (plasma), with the final goal of assessing the role of endotoxin adsorbed onto NPs in triggering inflammatory responses in human monocytes *in vitro*, a reliable and representative model system to assess the immunotoxic effects of NPs (Li et al. 2016).

Bacterial endotoxin can bind to the surface of Au NPs

Au10CIT were incubated with different concentrations of *E. coli* LPS at RT. A discrete red-shift of the SPR peak of the UV-VIS spectrum of few nm was observed, which indicates the binding of LPS to the Au NP surface (Figure 2). Since the citrate coating is loosely attached to the surface of Au NPs, it is easily replaced by other molecules in the solvent having higher affinity for the NP surface. Thus, once LPS was added, the replacement was already evident in

minutes, and seemed to reach a fairly stable condition in less than 1 h, with some peak vibrations observed afterwards and a tendency to increase at 1 and 3.3 µg/ml (Figure 2). Moreover, the increase in NP diameter and the decrease in Z-potential (Figure 3, center and right panels) indicated a dose-dependent binding of LPS onto the Au NP surface, which increased rapidly in the first 2 h (Figure 3 left panel, see also Figure 2), then slowly until 24 h and became apparently stable afterwards. After 24 h, the stability of the UV-VIS signal indicated a saturated Au NP surface (Figure 3, left panel), while the evolution of the DLS and Z-potential signals would indicate compaction and reorganization of the LPS coating layer (Figure 3, center and right panels). No aggregation of the NPs was observed during the course of the experiments. To further confirm that LPS can attach to the surface of 10 nm Au NPs, the Au10CIT were washed (centrifugation/resuspension) with endotoxin-free pure water. Unsurprisingly, the

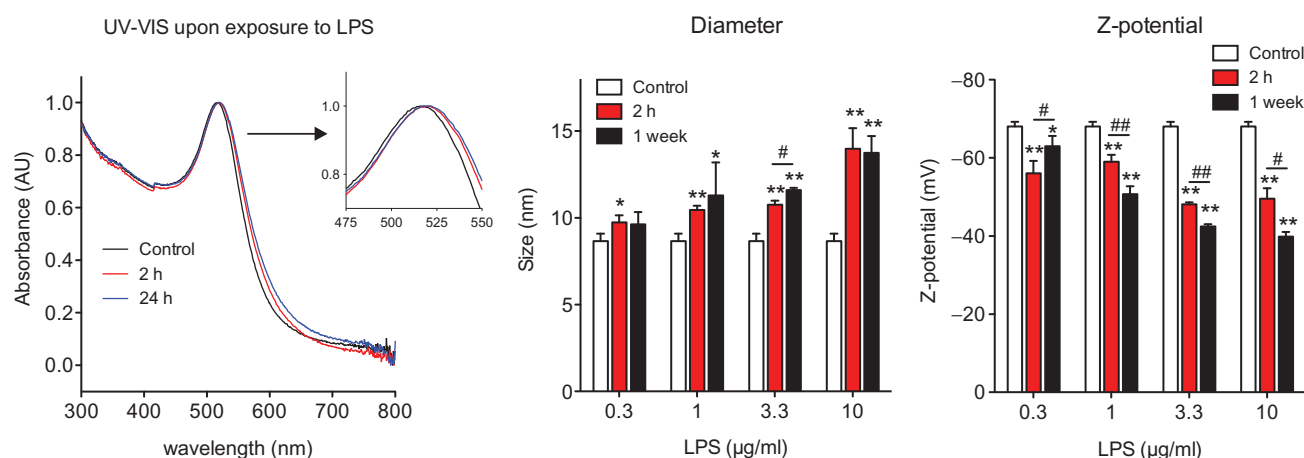


Figure 3. Characterization of Au10CIT after exposure to LPS. Left: UV-VIS spectrum characteristics after NP incubation with 1 µg/ml LPS; center: DLS; right: Zeta-potential. * $p < 0.05$, ** $p < 0.01$ (treated vs. control); # $p < 0.05$, ## $p < 0.01$ (2 h vs. 1 week incubation).

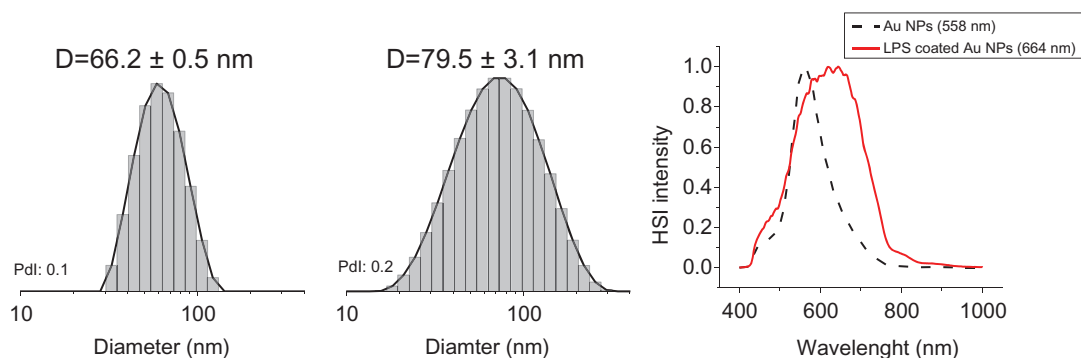


Figure 4. Characterization of Au40CIT after exposure to LPS. Size distribution of the intensity obtained from DLS measurements of Au NPs (left) and LPS-coated Au NPs (center) resulting in a calculated size difference of 13.3 nm. The presence of LPS on the NP surface is evident by analysis of the hyperspectral images obtained by dark-field microscopy (right). HSI intensity = hyperspectral imaging intensity in dark-field microscopy.

presence of LPS on the NP surface stabilized them, as they did not aggregate after the washing, in contrast to LPS-free sodium citrate-stabilized NPs that showed significant aggregation after resuspension in endotoxin-free water (Figure S1). These results confirm that the endotoxin is adsorbed on the surface of Au NPs.

The adsorption of LPS onto the surface of larger particles was tested by incubating Au40CIT with LPS. As shown in Figure 4, the presence of a saturated layer of LPS bound to the NP surface (defined as LPS corona) was verified by DLS and CytoViva. The diameter of the LPS-coated Au NP, measured by DLS, increased compared to the untreated Au NPs (Figure 4, left and center). The optical and hyperspectral imaging showed a clear wavelength shift upon LPS binding to the NPs (Figure 4, right panel).

To examine how different surface functionalization may change the LPS adsorption, the binding of

LPS to 40 nm and 80 nm Au NPs coated with deprotonated lipoic acid (Au40LIP and Au80LIP) was evaluated. Au40LIP and Au80LIP were incubated with different concentrations of LPS and their diameters were monitored over time as shown in Figure S2. A LPS dose-dependent NP size increase was observed, which occurred rapidly within 2 min after addition of LPS. It is likely that LPS at low concentrations cannot easily displace the tightly attached lipoic acid from the NP surface. The LPS coating with Au40LIP was also evident in the TEM micrographs (Figure S3).

Computational simulation and mathematical relationship between LPS and Au NPs

LPS binding to the surface of Au NPs was further studied by computational simulation in order to evaluate the quantitative relationship between LPS

and Au NPs, and the correlation of the UV-VIS SPR red-shift with the amount of LPS attached to the NP surface. An agent-based model (ABM) was applied to simulate the interactions between LPS and Au NPs *in silico* (Bonabeau 2002; Bachman and Sorger 2011). The simulation interface was a 601×601 2D grid generated in NetLogo, which was designed to simulate an environment of binding between LPS and Au NPs. Au NP number was initialized to 5 counts upon consideration of computational capability. LPS numbers were adjustable based on various LPS concentrations and Au NP numbers. Considering an average molecular weight (MW) for LPS of about 20 kDa and the nominal average density of LPS of 1.44 g/cm^3 (see Supporting Information reference 2), a 10 nm^2 LPS fingerprint was calculated (supporting info, Table S1, Figures S4 and S5). Therefore, the number of LPS molecules on the surface of a single 10 nm Au NP at saturating concentrations is 628 (see Supporting Information). In this simulation, it is assumed that the movement of LPS and Au NPs follows pure Brownian motion and therefore the movement for each LPS and Au NPs was updated per simulation step based on a uniform distribution with a range of (0, 360). Likewise, at each simulation step, the locations of LPS and Au NPs were updated based on the direction and moving step. The binding process occurs when a LPS molecule and an Au NP (or LPS-Au NP complex) occupy the same location in the simulation interface. At that specific location if on the Au NP surface there is room for binding (as stated above, assume one 10 nm Au NP can bind a maximum of 628 LPS molecules), the free LPS molecule will bind to this specific Au NP. Otherwise, LPS will move away to meet the adjacent Au NP. Once LPS binds to an Au NP, an LPS-Au NP complex is formed and the two entities move simultaneously in the next simulation step. The simulation terminates once all the Au NPs reach their maximal binding capacity (surface saturation). Thirty replicated runs for each LPS concentration were performed *in silico* and a statistical analysis was conducted using the software R 3.1.2 (<https://cran.r-project.org/bin/windows/base/old/3.1.2/>). As depicted in Figure 5 (upper panel), a correlation was observed between the initial LPS concentration and the saturation time ($p < 0.05$), which is consistent with the experimental observations in Figure 2. A video was produced in Netlogo,

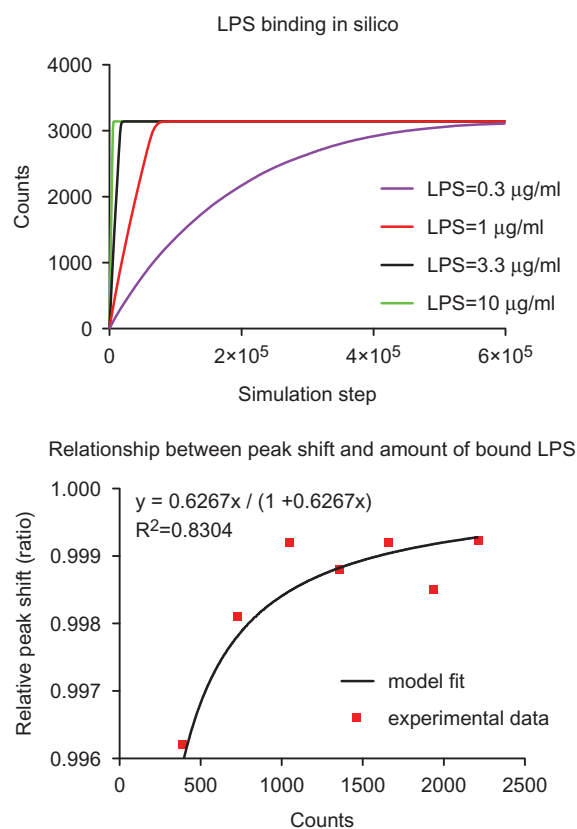


Figure 5. Computational simulation and mathematical relationship between LPS and Au NPs. Upper panel: Agent-based model (ABM) simulation between LPS and Au10CIT *in silico*. Lower panel: A mathematical relationship between the measured UV-VIS surface plasmon resonance (SPR) peak red-shift (red dots) and simulated amount of LPS bound on the surface of Au NPs was estimated using the Curve Fitting ToolBox in MatLab. On the Y axis is reported the relative peak shift (defined as SPR peak red-shift/maximum SPR peak red-shift). The maximum SPR red-shift was 520 nm in our experiments. The X axis is the amount of LPS bound onto Au NPs that was acquired *in silico*. The estimated curve follows a Langmuir absorption isotherm.

simulating the binding process between LPS and Au NPs (see Supporting Materials, videos 1 and 2). A statistically significant correlation was found between the SPR red-shift of the UV spectra of the formed LPS-Au NP complexes and the amount of bound LPS (Figure 5 lower panel). This indicates that the experimental data on red-shift are statistically correlated (Sum Square Error: 1.255×10^{-6} , R-square: 0.8304, adjusted R-square: 0.8304, root-mean-square deviation: 0.0004573) to the following the Langmuir absorption isotherm:

$$\frac{\lambda}{\lambda_{\max}} = \frac{K_{\lambda} \text{LPS}}{1 + K_{\lambda} \text{LPS}}$$

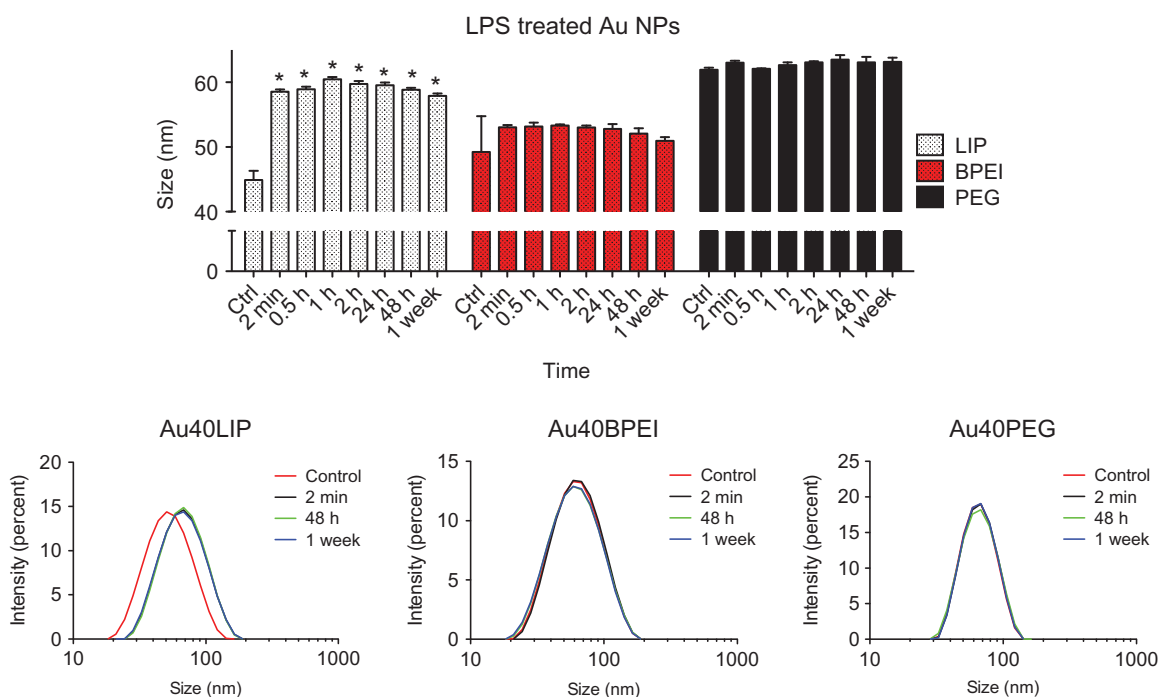


Figure 6. NP surface coating affects LPS-binding. Forty nm Au NPs with different surface coatings (LIP, BPEI and PEG) were incubated with 10 $\mu\text{g/ml}$ LPS for different times. Upper panel: time-dependent size variations measured by dynamic light scattering (DLS). Lower panels: size distribution variations of Au NPs before and after incubation with LPS. * $p < 0.01$ (treated vs. control).

In the equation above, λ represents SPR red-shift and λ_{max} represents the maximum observed SPR red-shift (520 nm in our experiments). LPS denotes the amount of LPS bound onto the NP surface *in silico*, and K_{λ} is an equilibrium constant for LPS binding to the NP surface. Using the Curve Fitting Tool in MATLAB, the estimated K_{λ} is 0.6267 (with 95% confidence limits of 0.4926, 0.7608).

Surface coating of Au NPs affects LPS binding

Binding of LPS was also assessed on Au NPs coated with different molecules, in addition to lipoic acid. Au40BPEI and Au40PEG were exposed to LPS at RT for different times and LPS binding was assessed by DLS in comparison with Au40LIP. As shown in Figure 6, only the Au40LIP showed a size increase upon LPS treatment, but no increase in size or variation was evident for Au40BPEI or Au40PEG over one week of incubation with LPS. These results show that different surface coatings can allow or avoid LPS binding to the NP surface. Highly soluble and large molecules such as PEG and BPEI provide steric repulsion to the NP surface preventing LPS binding, whereas lipoic acid (a stiff small molecule with hydrophilic and hydrophobic domains that makes dense self-assembled monolayers onto the

NP surface) does not provide steric repulsion and therefore allows for the binding of LPS.

LPS coating interfere with biomolecular corona formation on the Au NP surface

Formation of a biomolecular corona on the NP surface, upon interaction with biological fluids, is very important in determining the NP biological effects *in vitro* and *in vivo* (Casals et al. 2010; Monopoli et al. 2011; Salvati et al. 2013). Therefore, we investigated whether the presence of LPS (as unintentional contaminant) on the NP surface could alter the interaction between NPs and proteins and other molecules present in biological fluids. In Figure S6, the mean size of Au NPs in the presence or absence of LPS coating did not vary much after incubation in human plasma, but differences could be detected in the size distributions of LPS-coated vs. uncoated NPs, and these differences can be attributed to a stabilizing effect of LPS on NPs (as suggested by the data in Figure S1), and by the different properties of the NP-biomolecule complex.

We further analyzed if the LPS coating could affect the formation of a stable hard corona on the surface of NPs *in vitro*. The results shown in Figure 7 indicate a smaller increase in the size of Au

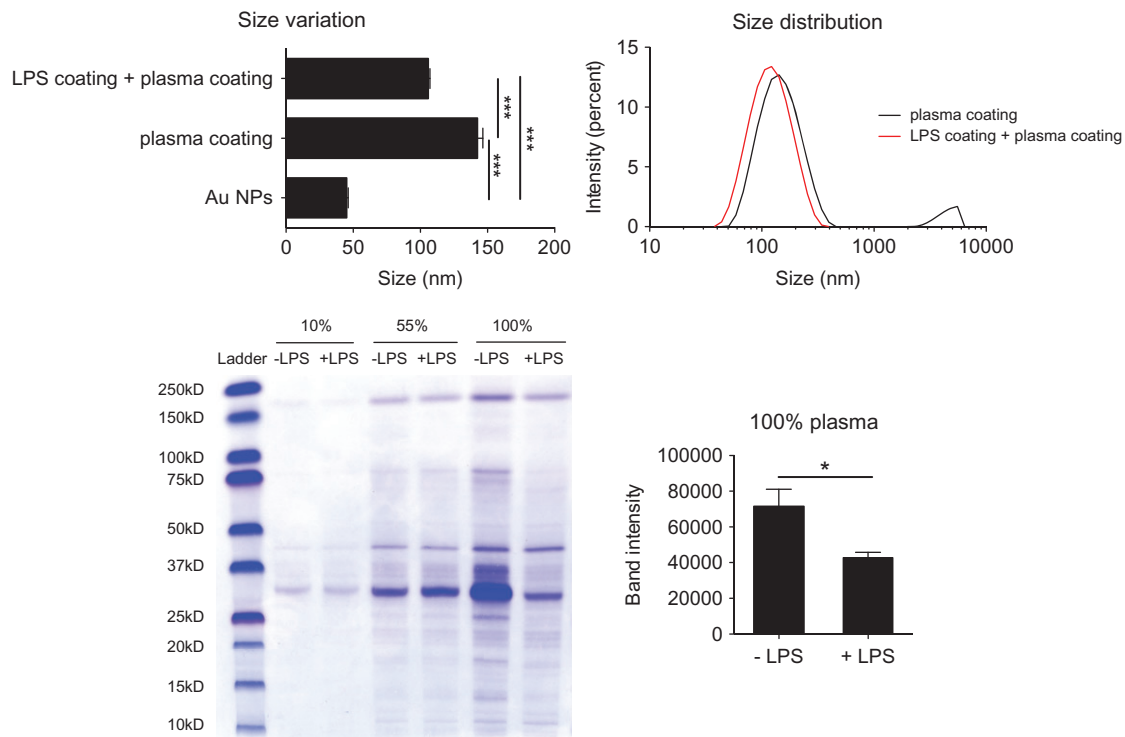


Figure 7. LPS binding to the NP surface interferes with the formation of a stable biomolecular corona. LPS-coated and uncoated Au40LIP were incubated with 100% human plasma at 37 °C for 4 h and washed with PBS to remove the loose biomolecular corona. Upper left: size variation, $***p < 0.001$; upper right: size distribution. LPS-coated and uncoated Au40LIP were incubated with 10%, 55%, and 100% human plasma at 37 °C for 4 h and washed with PBS. Human plasma proteins adsorbed on the NP surface were analyzed by SDS-PAGE. Lower left: SDS-PAGE gel; lower right: total band intensity of proteins recovered from LPS-coated and uncoated Au40LIP incubated with 100% human plasma. The results are the mean \pm SD of data obtained from two different samples. $*p < 0.05$.

NPs if the particles were pre-coated with LPS. Furthermore, the SDS-PAGE analysis showed a significant decrease in the biocorona formation on the surface of LPS-coated Au NPs, this finding being particularly evident upon incubation with undiluted human plasma (100%). It is apparent that many low MW proteins did not attach to the surface of LPS-coated Au NPs. This is consistent with the DLS size distribution data in Figure S6 which showed the small peak (possibly representing the low MW proteins) disappearing in LPS-coated Au NPs. Thus, the LPS coating, like PEG and BPEI, seems to make particles unable to adsorb plasma biomolecules in a stable fashion, likely by steric hindrance.

LPS coating on Au NPs induces inflammatory responses *in vitro*

LPS has potent inflammatory effects *in vivo* and *in vitro*, and activates innate/inflammatory cells, such as monocytes and macrophages, mainly through the TLR4 signaling pathway, a key mechanism of

the defensive inflammatory response against bacteria (Janeway and Medzhitov 2002, Murphy 2012). Therefore, the ability of LPS-coated Au NPs to induce inflammatory activation was tested in human primary monocytes *in vitro*. Results in Figure 8 showed that LPS-coated Au10CIT induced the expression of the *IL1B* gene and the production of the mature IL-1 β protein, suggesting that LPS-coated NPs not only upregulate the *IL1B* gene but could also activate the inflammasome-dependent IL-1 β maturation (Latz 2010). LPS-uncoated Au10CIT were unable to induce either *IL1B* gene expression or IL-1 β protein production. It was interesting to see that free LPS could induce, as expected, the expression of the *IL1RN* gene and the production of the anti-inflammatory cytokine IL-1Ra, the receptor antagonist of IL-1 β (Figure 8). However, the LPS-coated Au10CIT had little to no effect on both the *IL1RN* gene expression and IL-1Ra production, similarly to the uncoated Au10CIT (Figure 8, right panels). Thus, LPS-coated Au10CIT seem to display similar effects as free LPS in terms of inflammatory

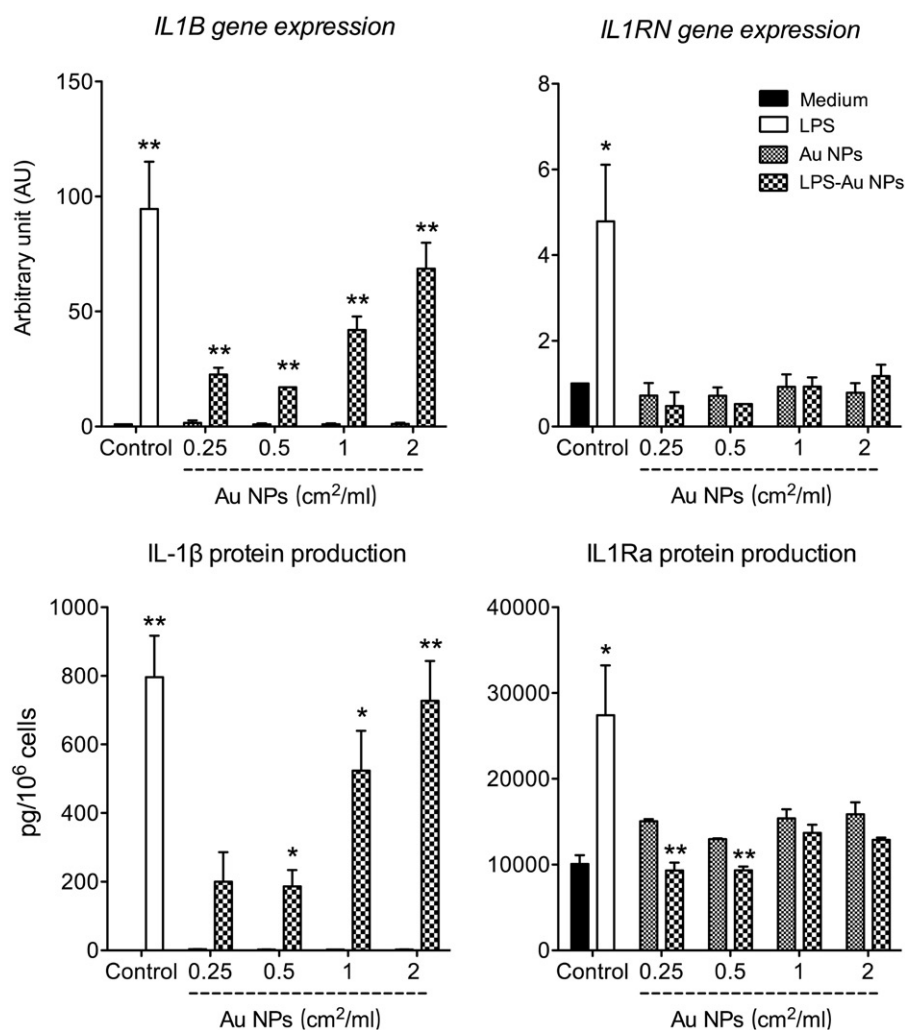


Figure 8. LPS-coated Au NPs induce inflammatory activation of human monocytes. Au10CIT were incubated with 200 ng/ml of LPS for 1 h. Unbound LPS was washed off, and the effects of LPS-coated Au NPs were assessed on human primary monocytes after 18 h incubation, in comparison with those triggered by 1 ng/ml LPS. Upper panels: expression of *IL1B* and *IL1RN* genes. Lower panels: production of the IL-1 β and IL-1Ra cytokines. The results are the mean \pm SD of data obtained from one experiment representative of 3 performed. * $p < 0.05$, ** $p < 0.01$ (LPS-coated vs. uncoated NPs).

cytokine production. However, this was not combined with the concomitant induction of anti-inflammatory effects. The differences in the mechanisms of IL-1 vs. IL-1Ra induction by LPS are still unexplored and are an area of ongoing research. In any case, we have evidence that, at the time point under study, LPS bound onto the NP surface can induce an inflammatory cytokine but not its anti-inflammatory inhibitor, thus LPS-coated Au NPs represent a new entity with an activity profile that is different from those of the two components. It is important to mention that both LPS-coated and uncoated NPs in these experiments were incubated with human serum to allow for the corona formation before administering them to the monocytes in culture. Thus, the different biological effects and

activity profiles between LPS-coated and uncoated NPs should include their different capacity of forming a biomolecular corona.

This observation was extended by testing the cell-activating capacity of LPS-coated and uncoated Au40CIT. Since these commercial NPs are contaminated with endotoxin, we decided to test them on a specifically designed LPS-responsive reporter cell line, which shows a dose-dependent reactivity to LPS that does not go into saturation at such LPS concentrations as in the case of primary human monocytes (exquisitely sensitive to LPS (Schwarz et al. 2014; Li and Boraschi 2016)). With this cell line and with an extensive dose-response experiment, it should be possible to distinguish between activation due to the original LPS contamination

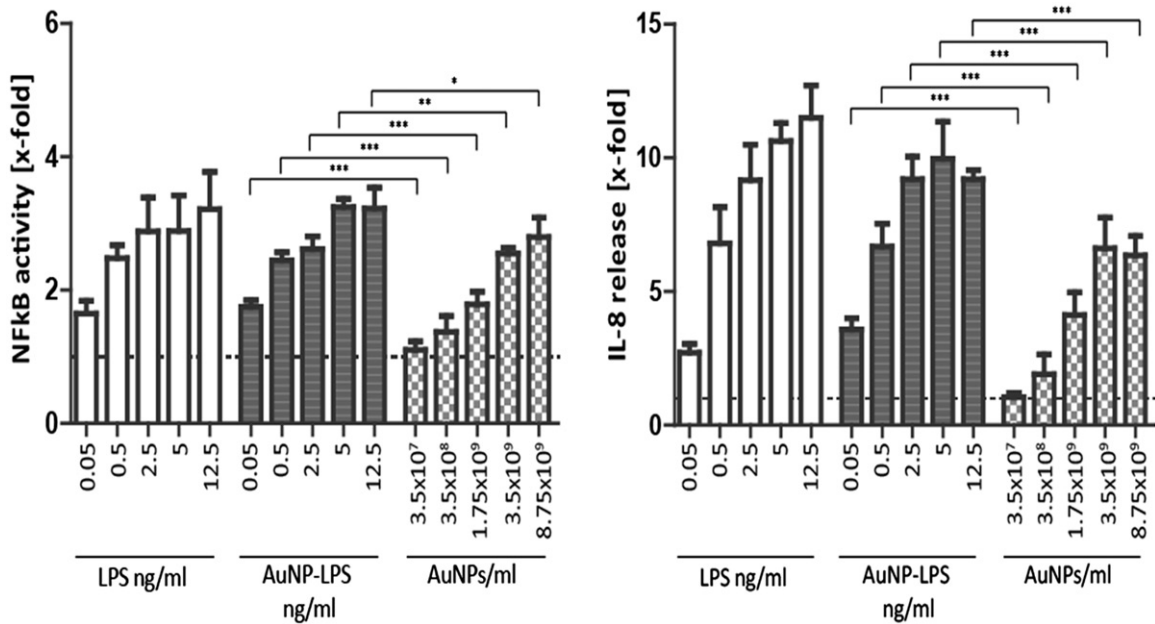


Figure 9. Activation of reporter HEK293 cells with free vs. NP-bound LPS. HEK293 cells transiently overexpressing TLR4, CD14, and MD2 were transfected with an NFκB-responsive LUC reporter gene. Left panel: NFκB activity was measured in response to free LPS, to LPS-coated Au40CIT NPs (the amount of LPS used for coating is indicated), and to the corresponding number of NPs. NFκB activity was assessed by measuring LUC-dependent light emission. Right panel: Release of IL-8 in response to the same stimuli was detected by ELISA in the culture supernatants. Results are expressed as fold increase vs. the value in untreated cell cultures (= 1; indicated as dotted horizontal line), and presented as mean \pm SD of 3 independent experiments. Values were compared to the respective concentration, * p < 0.05, ** p < 0.001, *** p < 0.0001.

and that induced by LPS intentionally adsorbed onto the NP surface. This system is based on a transient co-transfection of HEK 293 cells with plasmids encoding the various molecules of the LPS receptor (TLR4, CD14, MD2) and with a reporter plasmid with the luciferase (LUC) gene under the control of an NFκB-responsive promoter. The transiently transfected cells were exposed to free LPS, Au40CIT and the LPS-coated Au40CIT for 24 h. The concentrations of free LPS used in this assay were set to match the amount of LPS used for coating the Au40CIT NPs. Data in Figure 9 show the response of transfected HEK 293 cells to LPS-coated NPs is greater than that to uncoated NPs both in terms of NFκB activation and the induction of the inflammatory chemokine IL-8. Note that the uncoated NPs induced a response, as expected because of the initial contamination of these NPs with endotoxin. In fact, the extent of activation induced by contaminated NPs compares quite well with the response induced by corresponding LPS concentrations (the initial particle contamination roughly corresponds to 0.002, 0.02, 0.1, 0.2 and 0.5 ng/ml, as determined by the LAL assay). Hence, no difference occurred in the

activation capacity of LPS, either free or bound to NPs, at least in terms of NFκB activation and IL-8 production.

Discussion

The biological effects of engineered nanomaterials are a topic of considerable debate and important for nanomaterials' safety assessment. Contamination of NPs with bioactive molecules can significantly alter the NP biological effects. Therefore, it calls for the need of determining the type and grade of contamination, in order to define the true nano-effects (Dobrovolskaia et al. 2008). Despite the fact that nanomaterials have a tendency to interact with different biomolecules, studies determining the contamination of nanomaterials with different bacterial substances are limited. Endotoxin (LPS), an ubiquitous thermo-resistant toxin of bacterial origin, can cause various life-threatening diseases at low doses and can easily contaminate NPs, if the synthesis conditions are not well-controlled or handling processes are not adequately performed (Li and Boraschi 2016). In this study, the capacity of LPS to bind to the surface of Au NPs and how the presence of LPS

may alter the biological effects of NPs was investigated.

NP surfaces adsorb a wide range of molecules from the surrounding milieu to reduce their free energy, due to the highly reactive nature of their surface (Li and Boraschi 2016). Endotoxin is one of the unintentional contaminants that can be present on the surface of nanomaterials. In this study, LPS can easily bind to the surface of sodium citrate and lipoic acid coated Au NPs, and this binding capacity appears to be rapid and strong. For example, in the case of Au10CIT, the UV-VIS SPR peak red-shift results (Figure 2) indicate that binding of LPS occurs after 2 min at RT and reaches stability after approximately 1 h. The LPS-binding capacity appeared to be dose-dependent but temperature-independent, displaying essentially similar binding kinetics at 4 °C, representing the storage conditions, and 37 °C, representing biological conditions (data not shown). The corona formed by LPS on Au NPs was visualized by TEM (Figure S3).

Different coatings were investigated for Au NPs in this study, including sodium citrate, lipoic acid, BPEI, and PEG, which determine differences in surface chemistry, charge, and steric conditions. The interaction between citrate anions and the surface of Au NPs is weak, which makes it easy replacing the citrate ions with other molecules in the milieu, such as LPS. The binding of LPS was also observed on Au NPs with a tight coating, such as lipoic acid, which is deprotonated (negatively charged) at physiological pH (Figure S2 and S3). Lipoic acid forms a dense self-assembled “hard” monolayer onto the NP surface. However, when using BPEI (positively charged at physiological pH) or PEG (neutral), no LPS absorption was observed, consistent with the reason why these molecules are used to avoid NP opsonization (Owens and Peppas 2006). Note that the differences in surface charge were not as important as the steric repulsion provided by the polymeric coating molecules. Surface charges have relevance in physiological media, due to the presence of high electrolyte concentrations, therefore they are expected to have an effect on the NP-LPS aggregation rate but not a fundamental effect on the formation of a biomolecular corona. Thus, from these results, it is evident that LPS binding to NPs varies depending on the surface coating and charge.

In the attempt to understand the quantitative relationship between LPS and Au NPs, and the correlation of the SPR red-shift with the amount of LPS binding to the Au NPs surface, ABM was applied to simulate *in silico* the interactions between LPS and Au NPs. ABM inherently captures repetitive spatial interactions between agents in a stochastic process or under a known probability distribution, making it a powerful tool to render valuable information and simulate a complex system. Monitoring the SPR red-shift by time until Au NPs reached binding saturation was found to depend on the initial LPS concentration, a finding consistent between the ABM and our experimental data. After calibrating the mathematical relationship between UV-VIS SPR red-shift and the amount of LPS bound on Au NPs, using simulated and experimental data, a mathematical relationship was obtained that followed a Langmuir absorption isotherm. This finding further demonstrates that LPS-binding quantitatively correlates with the SPR red-shift of Au NPs.

The biomolecular corona that forms on the surface of NPs upon interaction with biological fluids is a very important phenomenon that affects the biological behavior of NPs (Lundqvist et al. 2008; Casals and Puntès 2012). Here, we have examined the formation of the biocorona onto NPs that have been contaminated with LPS, a molecule consisting primarily of lipids, carbohydrates, and importantly, being ubiquitous in nature and a common contaminant of NP preparations (Vallhov et al. 2006; Li and Boraschi 2016). It is reasonable to think that the LPS coating can interfere with a subsequent corona formation with molecules coming from biological fluids in *in vitro* or *in vivo* conditions. In this regard, we have investigated how the LPS coating on Au NPs could lead to anomalies in the formation of the biomolecular corona. We showed that the LPS coating on Au NPs has significant effects on size distribution after incubation with human plasma at 37 °C (Figures 7 and S6). This suggests that the presence of LPS on the NP surface causes a decrease of the available surface area and its free energy, thereby decreasing the interaction with plasma molecules. This also indicates a strong adherence of LPS to the NP surface and the inability of plasma molecules to displace it. By analyzing the amount and composition of proteins forming the biomolecular corona on the NP surface by SDS-PAGE, we showed that

the formation of the biocorona decreased significantly in LPS-coated vs. LPS-uncoated Au NPs (Figure 7). In addition, it seems the biocorona that forms on the surface of LPS-coated NPs preferentially contains high MW proteins, since apparently many low MW proteins were unable to attach to the LPS-coated NP surface. This implies that the biological properties of NPs can significantly change consequent to the change in the biocorona composition. This limited availability of the NP surface, due to the presence of LPS, may be of concern in preclinical studies for biomedical applications, as the unintentional presence of LPS in NP preparations may affect surface functionalization and consequent efficacy of nanodrugs. Therefore, the unwanted binding of LPS on the surface of NPs interferes with the formation of a biocorona, thereby causing additional variations in biological effects. Thus, the adsorption of LPS on the NP surface can be considered as an unintended modulation of the NP surface properties.

The inflammatory activity of LPS is mainly due to activation of the TLR4 signaling pathway in innate immune cells. Upon TLR4 activation, cells produce many inflammatory factors, including IL-1 β , a key inflammatory and immunostimulating cytokine (Dinarello 2009; Dinarello 2011; Joosten, Netea, and Dinarello 2013) and, as feedback mechanism, also anti-inflammatory factors such as the IL-1 inhibitor IL-1Ra. Since it is likely that an unintentional presence of LPS on the NP surface may lead to acquisition of LPS-dependent inflammatory effects, we studied how the presence of LPS coating may affect the biological effects of NPs. This was done by examining the ability of LPS-coated NPs to induce an inflammatory reaction in human monocytes *in vitro*. The results in Figures 8 and 9 show that the LPS coating could induce/increase significantly the inflammatory effects of Au NPs. This implies that the presence of LPS may lead to misinterpreting results concerning nanomaterial inflammatory potential, as LPS may be the sole responsible of the inflammatory response often attributed to NPs in *in vitro* and *in vivo* nanosafety studies in which the presence of LPS contamination was not assessed. However, while LPS-coated NPs could induce LPS-like inflammatory responses such as NF κ B activation and expression/production of inflammatory

cytokines such as IL-1 β and IL-8, it is notable that LPS-NPs were unable to reproduce the LPS-induced induction of anti-inflammatory mechanisms such as the expression/production of the IL-1 inhibitor IL-1Ra. The fact that LPS-coated NPs, at variance with free LPS, were unable to activate the anti-inflammatory feedback mechanisms (aiming at resolving inflammation in the context of a normal defensive response) suggests that adsorption of LPS on the NP surface alters its structure and/or orientation in a fashion that allows maintaining its inflammation-inducing capacity but that eliminates its inflammation-resolving effects. While there is no data discriminating between the two LPS activities in terms of receptor-binding modes, it should be noted that activation by LPS can occur in complex ways, with optimal activation involving soluble LBP and MD2, membrane TLR4 and CD14, and receptor clustering, but that activation can be obtained also in the absence of one or more of the co-receptor molecules. That LPS-coated NPs have the same inflammatory capacity of free LPS was confirmed also with a reporter cell-based system. These data imply that the altered biocorona does not influence the induction of LPS-mediated inflammation. On the other hand, it is possible that differences in the biocorona may take part in the inability of LPS-coated NPs to induce LPS-like anti-inflammatory activation. Overall, this means that LPS-coated Au NP represents new entities with an activity profile that is different from those of the two components, and in which the effects of LPS can be exacerbated.

Conclusion

In this study, the binding capacity between LPS, a bacterial-derived ubiquitous contaminant, and Au NPs was examined. The binding of LPS to the surface of Au NPs was significant and varied according to the NP surface functionalization. Coating with either citrate or lipoic acid (small molecules) allowed the formation of a stable LPS coating, whereas coating with bulky molecules such as BPEI and PEG provided enough steric repulsion to avoid LPS-binding. LPS-coated NPs have at least two characteristics that differ from uncoated NPs: the presence of LPS on their surface, and an anomalous biocorona,

composed by lower amounts of proteins, preferentially of high MW. How these changes influence the biological effects of NPs was tested on human primary monocytes and on transfected HEK 293 reporter cells *in vitro*. The data obtained suggest two conclusions. First, that non-inflammatory NPs may acquire inflammation-inducing capacity just by adsorbing LPS onto their surface. Second, that LPS-coated NPs are new entities, with a functional profile that differs from those of the two components. In particular, LPS-coated NPs appear to maintain the capacity of LPS to induce inflammatory responses (NF κ B activation, expression and production of IL-1 β and IL-8) but lose the ability of LPS to activate inflammation-resolving mechanisms (expression and production of the anti-inflammatory cytokine IL-1Ra).

These data suggest that unintentional adsorption of endotoxin to engineered NP surface can significantly affect the biomolecular corona formation and inflammatory/immunotoxic effects and, if going undetected, may lead to erroneous interpretation of nanotoxicity data. Distinguishing the true NP effects from those caused by biologically active contaminants such as LPS is key to a correct and reliable nanosafety and nano-bio-interaction evaluation. Another important conclusion is that adsorption of bioactive contaminants, such as LPS, from the environment, exposes human beings and environmental living species to new entities with a toxic potential that cannot be predicted from the toxicity of the individual components.

Supporting information

The Supporting Information is as follows: methods for estimation of the number of LPS molecules on the surface of Au NPs; Table S1: Size determination of LPS, Au NPs and LPS-Au NPs with DLS; Figure S1: Stability of LPS-coated Au NPs; Figure S2: LPS-induced size increase of lipoic acid-coated Au NPs; Figure S3: Transmission electron micrographs depicting LPS bound to lipoic acid-coated Au NPs; Figure S4: UV-VIS spectra of the LPS, Au NPs and LPS-Au NPs conjugates before and after centrifuge purification; Figure S5: Diagram showing the size increase of Au NPs after LPS coating. Figure S6: The presence of LPS on the NP surface interferes with the formation of a biomolecular corona upon

exposure to human plasma; Videos 1 and 2: NetLogo simulation of the 1 μ g/ml and 10 μ g/ml LPS-binding process to Au NPs.

Acknowledgements

This study was supported by the European Community's Seventh Framework Programme (FP7/2007-2013) projects NanoTOES (PITN-GA-2010-264506), NanoValid (GA 263147), and by the H2020 project PANDORA (GA H2020-MSCA-ITN-2015-671881), National Natural Science Foundation of China (31701005) and funds from the Nanotechnology Innovation Center of Kansas State University, Manhattan, KS. We thank Samuel M. Lawrence and Leslie Krauss from CytoViva Inc., and Hoffmann Goetz from Schaefer Technology GmbH, for conducting the hyperspectral images and analysis of LPS-coated and uncoated Au NPs. We thank Dr. Ngoc Tran (Institut Català de Nanotecnologia, Barcelona, Spain) for technical support, Mr. Ravi Thakkar (Kansas State University) for TEM support, and Min Li-Weber (DKFZ, Heidelberg, Germany), Andrei Medvedev and Douglas Golenbock (University of Massachusetts Medical School, Worcester, MA, USA) for providing NF κ B-LUC, TLR4, CD14, and MD2 plasmids.

Disclosure statement

Authors declare that they have no financial or non-financial competing interests.

ORCID

Yang Li  <http://orcid.org/0000-0001-7242-4687>
 Zhenzhen Shi  <http://orcid.org/0000-0001-9922-3957>
 Zhoumeng Lin  <http://orcid.org/0000-0002-8731-8366>
 Nancy A. Monteiro-Riviere  <http://orcid.org/0000-0002-0132-0861>
 Diana Boraschi  <http://orcid.org/0000-0002-3953-4056>

References

- Bachman, J. A., and P. Sorger. 2011. "New Approaches to Modeling Complex Biochemistry." *Nature Methods* 8: 130.
- Bastús, N. G., E. Casals, S. Vázquez-Campos, and V. Puentes. 2008. "Reactivity of Engineered Inorganic Nanoparticles and Carbon Nanostructures in Biological Media." *Nanotoxicology* 2: 99–112.
- Bastús, N. G., J. Comenge, and V. Puentes. 2011. "Kinetically Controlled Seeded Growth Synthesis of Citrate-Stabilized Gold Nanoparticles of up to 200 nm: Size Focusing Versus Ostwald Ripening." *Langmuir* 27: 11098–11105.
- Bonabeau, E. 2002. "Agent-Based Modeling: Methods and Techniques for Simulating Human Systems." *Proceedings of the National Academy of Sciences* 99: 7280–7287.
- Boraschi, D., and A. Duschl. 2012. Immune System. In *Adverse Effects of Engineered Nanomaterials*, edited by B. Fadeel, A.

- Pietroiusti, and A.A. Shvedova, 169–184. Amsterdam: Academic Press.
- Bromberg, L., E. P. Chang, C. Alvarez-Lorenzo, B. Magarinos, A. Concheiro, and T. A. Hatton. 2010. "Binding of Functionalized Paramagnetic Nanoparticles to Bacterial Lipopolysaccharides and DNA." *Langmuir* 26: 8829–8835.
- Casals, E., T. Pfaller, A. Duschl, G. J. Oostingh, and V. Puentes. 2010. "Time Evolution of the Nanoparticle Protein Corona." *ACS Nano* 4: 3623–3632.
- Casals, E., and V. F. Puentes. 2012. "Inorganic Nanoparticle Biomolecular Corona: Formation, Evolution and Biological Impact." *Nanomedicine* 7: 1917–1930.
- Choi, K., J. E. Riviere, and N. A. Monteiro-Riviere. 2016. "Protein Corona Modulation of Hepatocyte Uptake and Molecular Mechanisms of Gold Nanoparticle Toxicity." *Nanotoxicology* 11: 64–75.
- Darkow, R., T. Groth, W. Albrecht, K. Lützwow, and D. Paul. 1999. "Functionalized Nanoparticles for Endotoxin Binding in Aqueous Solutions." *Biomaterials* 20: 1277–1283.
- Dinarello, C. A. 2009. "Immunological and Inflammatory Functions of the Interleukin-1 Family." *Annual Review of Immunology* 27: 519–550.
- Dinarello, C. A. 2011. "Interleukin-1 in the Pathogenesis and Treatment of Inflammatory Diseases." *Blood* 117: 3720.
- Dobrovolskaia, M. A., P. Aggarwal, J. B. Hall, and S. E. Mcneil. 2008. "Preclinical Studies to Understand Nanoparticle Interaction with the Immune System and its Potential Effects on Nanoparticle Biodistribution." *Molecular Pharmaceutics* 5: 487–495.
- Dobrovolskaia, M. A., D. R. Germolec, and J. L. Weaver. 2009. "Evaluation of Nanoparticle Immunotoxicity." *Nature Nanotechnology* 4: 411–414.
- Ge, C., Y. Li, J. J. Yin, Y. Liu, L. Wang, Y. Zhao, and C. Chen. 2012. "The Contributions of Metal Impurities and Tube Structure to the Toxicity of Carbon Nanotube Materials." *NPG Asia Materials* 4: e32.
- Gorbet, M. B., and M. V. Sefton. 2005. "Endotoxin: The Uninvited Guest." *Biomaterials* 26: 6811–6817.
- Janeway, C. A., and R. Medzhitov. 2002. "Innate Immune Recognition." *Annual Review of Immunology* 20: 197–216.
- Joosten, L. A., M. G. Netea, and C. A. Dinarello. 2013. "Interleukin-1 β in Innate Inflammation, Autophagy and Immunity." *Seminars in Immunology* 25: 416–424.
- Latz, E. 2010. "The Inflammasomes: Mechanisms of Activation and Function." *Current Opinion in Immunology* 22: 28–33.
- Li, Y., and D. Boraschi. 2016. "Endotoxin Contamination: A Key Element in the Interpretation of Nanosafety Studies." *Nanomedicine* 11: 269–287.
- Li, Y., M. Fujita, and D. Boraschi. 2017. "Endotoxin Contamination in Nanomaterials Leads to the Misinterpretation of Immunotoxicity Results." *Frontiers in Immunology* 8: 472.
- Li, Y., P. Italiani, E. Casals, N. Tran, V. F. Puentes, and D. Boraschi. 2015. "Optimising the Use of Commercial LAL Assays for the Analysis of Endotoxin Contamination in Metal Colloids and Metal Oxide Nanoparticles." *Nanotoxicology* 9: 462–473.
- Li, Y., P. Italiani, E. Casals, D. Valkenburg, I. Mertens, G. Baggerman, I. Nelissen, V. Puentes, and D. Boraschi. 2016. "Assessing the Immunotoxicity of Engineered Nanoparticles with a Novel *In Vitro* Model Based on Human Primary Monocytes." *ACS Applied Materials & Interfaces* 8: 28437–28447.
- Li, Y., Y. Liu, Y. Fu, T. Wei, L. Le Guyader, G. Gao, R. S. Liu, Y. Z. Chang, and C. Chen. 2012. "The Triggering of Apoptosis in Macrophages by Pristine Graphene Through the MAPK and TGF- β Signaling Pathways." *Biomaterials* 33: 402–411.
- Li, Y., and N. A. Monteiro-Riviere. 2016. "Mechanisms of Cell Uptake, Inflammatory Potential and Protein Corona Effects with Gold Nanoparticles." *Nanomedicine* 11: 3185–3203.
- Li-Weber, M., M. Giasi, and P. H. Krammer. 1998. "Involvement of Jun and Rel Proteins in Up-Regulation of Interleukin-4 Gene Activity by the T Cell Accessory Molecule CD28." *Journal of Biological Chemistry* 273: 32460–32466.
- Lundqvist, M., J. Stigler, G. Elia, I. Lynch, T. Cedervall, and K. A. Dawson. 2008. "Nanoparticle Size and Surface Properties Determine the Protein Corona with Possible Implications for Biological Impacts." *Proceedings of the National Academy of Sciences* 105: 14265–14270.
- Monopoli, M. P., D. Walczyk, A. Campbell, G. Elia, I. Lynch, F. Baldelli Bombelli, and K. A. Dawson. 2011. "Physical-Chemical Aspects of Protein Corona: Relevance to *In Vitro* and *In Vivo* Biological Impacts of Nanoparticles." *Journal of the American Chemical Society* 133: 2525–2534.
- Murali, K., K. Kenesei, Y. Li, K. Demeter, Z. Környei, and E. Madarász. 2015. "Uptake and Bio-Reactivity of Polystyrene Nanoparticles is Affected by Surface Modifications, Ageing and LPS Adsorption: *In Vitro* Studies on Neural Tissue Cells." *Nanoscale* 7: 4199–4210.
- Murphy, K. M. 2012. *Janeway's Immunobiology*. 8th ed. New York: Garland Science.
- Netlogo. 2014. Netlogo. 5.1.0 ed. <https://ccl.northwestern.edu/netlogo/5.1.0/>
- Oostingh, G. J., E. Casals, P. Italiani, R. Colognato, R. Stritzinger, J. Ponti, T. Pfaller, Y. Kohl, D. Ooms, and F. Favilli. 2011. "Problems and Challenges in the Development and Validation of Human Cell-Based Assays to Determine Nanoparticle-Induced Immunomodulatory Effects." *Particle and Fibre Toxicology* 8: 8.
- Owens, D. E., and N. A. Peppas. 2006. "Opsonization, Biodistribution, and Pharmacokinetics of Polymeric Nanoparticles." *International Journal of Pharmaceutics* 307: 93–102.
- Peula-García, J., J. Molina-Bolivar, J. Velasco, A. Rojas, and F. Galisteo-González. 2002. "Interaction of Bacterial Endotoxins (lipopolysaccharide) with Latex Particles: Application to Latex Agglutination Immunoassays." *Journal of Colloid and Interface Science* 245: 230–236.
- Pfaffl, M. W. 2001. "A New Mathematical Model for Relative Quantification in Real-Time RT-PCR." *Nucleic Acids Research* 29: e45.
- Salvati, A., A. S. Pitek, M. P. Monopoli, K. Prapainop, F. B. Bombelli, D. R. Hristov, P. M. Kelly, C. Åberg, E. Mahon,

- and K. A. Dawson. 2013. "Transferrin-Functionalized Nanoparticles Lose Their Targeting Capabilities when a Biomolecule Corona Adsorbs on the Surface." *Nature Nanotechnology* 8: 137–143.
- Savolainen, K., U. Backman, D. Brouwer, B. Fadeel, T. Fernandes, T. Kuhlbusch, R. Landsiedel, I. Lynch, and L. Pylkkänen. 2013. *Nanosafety in Europe 2015-2025: Towards Safe and Sustainable Nanomaterials and Nanotechnology Innovations*. Helsinki: Finnish institute of occupational Health.
- Schwarz, H., M. Schmittner, A. Duschl, and J. Horejs-Hoeck. 2014. "Residual Endotoxin Contaminations in Recombinant Proteins are Sufficient to Activate Human CD1c + Dendritic Cells." *PloS One* 9: e113840.
- Shi, Z., S. K. Chapes, D. Ben-Arieh, and C.-H. Wu. 2016. "An Agent-Based Model of a Hepatic Inflammatory Response to Salmonella: A Computational Study Under a Large Set of Experimental Data." *PloS One* 11: e0161131.
- Shi, Z. Z., C.-H. Wu, and D. Ben-Arieh. 2014. "Agent-Based Model: A Surging Tool to Simulate Infectious Diseases in the Immune System." *Open Journal of Modelling and Simulation* 2: 12–22.
- Turkevich, J., P. C. Stevenson, and J. Hillier. 1955. "A Study of the Nucleation and Growth Processes in the Synthesis of Colloidal Gold." *Discussions of the Faraday Society* 11: 55–75.
- Vallhov, H., J. Qin, S. M. Johansson, N. Ahlborg, M. A. Muhammed, A. Scheynius, and S. Gabrielsson. 2006. "The Importance of an Endotoxin-Free Environment During the Production of Nanoparticles Used in Medical Applications." *Nano Letters* 6: 1682–1686.
- Wang, P., X. Nie, Y. Wang, Y. Li, C. Ge, L. Zhang, L. Wang, et al. 2013. "Multiwall Carbon Nanotubes Mediate Macrophage Activation and Promote Pulmonary Fibrosis Through TGF- β /Smad Signaling Pathway." *Small* 9: 3799–3811.